California reanalysis downscaling at 10 km using an ocean-atmosphere coupled regional model system

Haiqin Li,[1,2] Masao Kanamitsu,[1] and Song-You Hong[3]

[1]   A fully coupled regional downscaling system based on the Regional Spectral Model (RSM) for atmosphere and the Regional Ocean Modeling System (ROMS) for the ocean was developed for the purpose of downscaling observed analysis or global model outputs. The two models share the same grid and resolution with efficient parallelization through the use of dual message passing interfaces. Coupled downscaling was performed using historical Simple Ocean Data Assimilation (SODA) oceanic reanalysis and NCEP/DOE (R-2) atmospheric reanalysis in order to study the impact of coupling on the regional scale atmospheric analysis. The results were subsequently compared with the uncoupled downscaling forced by the prescribed observed sea surface temperature (SST). The coupled experiment yielded the SST and ocean current with realistic small-scale oceanic features that are almost absent in the oceanic reanalysis. Upwelling over the California coast is well resolved and comparable to findings obtained from high-resolution observations. The coupling impact on the atmospheric circulation mainly modulates the near surface atmospheric variables when compared to the simulation conducted without coupling. The duration of the Catalina Eddy detected in the coupled experiment increased by about 6.5% when compared to that in the uncoupled experiment. The offshore land breeze is enhanced by about 10%, whereas the change in the onshore sea breeze is very small during the summer.

1.   Introduction

[2]   Since the first successful demonstrations of regional climate modeling by *Dickinson et al.* [1989] and *Giorgi and Bates* [1989], regional climate models (RCMs) have been widely used to downscale global reanalysis and general circulation model (GCM) outputs. This dynamical downscaling allows high resolution results to be obtained from coarse resolution driving data for various purposes, such as long-term reanalysis downscaling [*Liang et al.*, 2004; *Kanamitsu and Kanamaru*, 2007], the downscaling of projected climate scenarios [*Giorgi et al.*, 1994; *Leung et al.*, 2004; *Stowasser et al.*, 2007; *Hong et al.*, 2010], seasonal prediction [*Sun et al.*, 2006], process studies identifying soil moisture atmosphere interactions [*Kanamitsu and Mo*, 2003], analyses on the effects of snow on the Asian summer monsoon

[*Seol and Hong*, 2009; *Souma and Wang*, 2009], and an evaluation of physics parameterization schemes [*Yhang and Hong*, 2008; *Koo and Hong*, 2010]. Such an approach is also useful to isolate regional feedback imbedded within evolving large-scale features [*Hong and Kalnay*, 2000]. It should be noted that the above cited RCM studies use the sea surface temperature (SST) derived from either observation or GCM forecasts.

[3]   It is well known that a correct representation of the SST in atmospheric models is crucial to achieve realistic interactions between the ocean and atmosphere. The ocean and atmosphere exchange energy, momentum, and mass at the sea surface. The heating or cooling of the SST alters the atmospheric circulation, surface heat fluxes, and wind stress, which in turn modify the ocean thermal structure and circulation in an ocean-atmosphere coupled system. While this type of fully coupled system, known as an Atmosphere-Ocean General Circulation Model (AOGCM), has been widely applied in global model communities to study climate change [e.g., *Russell and Rind*, 1999; *Held and Soden*, 2006; *Vecchi and Soden*, 2007] and seasonal forecasts [e.g., *Kirtman*, 2003; *Saha et al.*, 2006], it is not commonly used for regional modeling communities. Most regional model studies utilize ocean temperature data derived from either observation or a global model coupled simulation. The typical resolution of the SST data ranges from 100 to 200 km, which is much coarser than the RCM grid.

[1]Scripps Institution of Oceanography, University of California, San Diego, California, USA.
[2]Center for Ocean-Atmosphere Prediction Studies, Florida State University, Tallahassee, Florida, USA.
[3]Department of Atmospheric Sciences, College of Science, Yonsei University, Seoul, South Korea.

Corresponding author: S.-Y. Hong, Department of Atmospheric Sciences, College of Sciences, Yonsei University, Seoul 120-749, South Korea. (shong@yonsei.ac.kr)

[4] The application of high-resolution regional coupled ocean-atmosphere models has been attempted in recent years. Using the Scripps Coupled Ocean-Atmosphere Regional (SCOAR) model, *Seo et al.* [2007a, 2007b] showed that a coupled regional model is capable of reproducing many mesoscale ocean-atmosphere interaction features from observation. *Xie et al.* [2007] coupled a regional climate model with a basin scale oceanic general circulation model, and reproduced salient features of eastern Pacific climate on both the basin and mesoscales. *Boé et al.* [2011] used the University of California, Los Angeles (UCLA)/Joint Institute for Regional Earth System Science and Engineering (JIFRESSE) Mesoscale Coupled Model (UMCM), which couples the Regional Ocean Modeling System (ROMS) with the Weather Research and Forecasting Model (WRF), to study the respective roles of orography and SST/wind links in the mesoscale spatial variability of wind in the California upwelling region. The researchers found that orographic effects are dominant within about 150 km of the coast. Such findings suggest the importance of coupling ocean and atmospheric models in high-resolution RCMs.

[5] California Reanalysis Downscaling at 10 km (CaRD10) [*Kanamitsu and Kanamaru*, 2007, hereinafter KK07] from 1948 to 2005 was conducted with the Regional Spectral Model (RSM) [*Juang and Kanamitsu*, 1994; *Juang et al.*, 1997] and was recently extended to the year 2011. CaRD10 produced regional-scale features that were better than those from the coarse resolution reanalysis used to force the regional model, and comparable to those from the North American Regional Reanalysis (NARR) [*Mesinger et al.*, 2006]. However, CaRD10 has a positive bias in precipitation for heavy precipitation events, and does not adequately reproduce the southwestern monsoon over the Gulf of California due to the lateral boundary position [*Kanamaru and Kanamitsu*, 2007]. CaRD10 has been used for oceanic and atmospheric research and applications [*Song et al.*, 2011; *Kanamitsu and DeHaan*, 2011].

[6] The ROMS has been extensively applied to study various phenomena of the California Current System, and has been used in successful simulations of long-term variability [*Marchesiello et al.*, 2003; *Di Lorenzo et al.*, 2005; *Centurioni et al.*, 2008; *Song et al.*, 2011]. Heat flux correlation was employed in these ROMS applications.

[7] The RSM and ROMS were coupled in the SCOAR model, which is a research-oriented model developed without much consideration for practical application. In this study, we developed a fully coupled regional ocean-atmosphere model system for practical applications. The starting point of this coupled system is the SCOAR model, but with several key differences in the new coupled system. In the new framework, the RSM and ROMS are the regional atmosphere and ocean components, respectively, of the ECPC G-RSM modeling system (http://g-rsm.wikispaces.com/). The update of the standalone RSM and ROMS will be automatically updated for the coupled model. The SCAOR oceanic MATLAB preprocessing programs were completely converted to Fortran programs in the RSM-ROMS. The wind stress and heat flux are calculated via a bulk formula in the SCOAR model, while the fluxes are directly computed from the RSM in the new framework. Rather than using sequential coupling for the SCOAR model, the more efficient MPI dual coupling scheme is adopted by RSM-ROMS. Interpolation between ocean and atmosphere grids is desirable for the SCOAR model, but the same model domain and grid resolution are devised for RSM-ROMS. Oceanic climatology forcing is used in the SCOAR [*Seo et al.*, 2007a, 2007b] model, while observed or GCM-simulated time-varying oceanic initial and boundary forcing are incorporated by RSM-ROMS for practical application to weather and climate forecasts.

[8] Recent studies based on satellite observations conducted over the region of the California Current System (CCS) suggest that there is tight coupling between summertime SST gradients and wind stress derivatives [*Chelton et al.*, 2007; *Chelton and Xie*, 2010]. The new system developed in this study will be used to identify the coupling effect of the California coastal area, which is absent in KK07. A 12-year downscaling at a 10-km resolution over California is presented in this paper. The oceanic state of the coupled downscaling is verified against various observations. The atmospheric climatology difference between coupled and uncoupled experiments is examined, together with mesoscale ocean-atmosphere interactions along the coast. It should be emphasized that the analysis in this paper is focused on the region over the California coastal area.

[9] The coupled modeling system and experiment design are described in section 2, while an evaluation of the model results are presented in section 3. Changes in the atmospheric climatology due to coupling are discussed in section 4, and an examination of the mesoscale circulation impact is outlined in section 5. Concluding remarks are ultimately presented in section 6.

2. Modeling System and Experiment Design

2.1. Regional Spectral Model (RSM)

[10] The RSM is used as the atmospheric part of the coupling system. This model has been extensively used for dynamical downscaling and operational short-range forecasting. The RSM uses a spectral method (with sine and cosine series) in two dimensions [*Juang and Kanamitsu*, 1994]. A unique aspect of the model is that spectral decomposition is applied to the difference between the full field and the time-involving background global analysis field. This difference is denoted as perturbation, and the background global analysis is called the base. The horizontal derivatives that appear in the dynamical forcing terms in the prediction equations are first computed so as to yield the perturbation spectral coefficients and the base field separately. The derivatives are then summed to obtain the total forcing.

[11] The model equations consist of a momentum equation, a thermodynamic equation, a mass conservation equation, and a moisture equation. A primitive equation system, in which vertical motion is diagnosed rather than predicted, is employed in this work. A nonlocal boundary layer scheme [*Hong and Pan*, 1996] is also used. The four-layer Community Noah land surface scheme (Noah LSM) [*Chen and Dudhia*, 2001] is utilized rather than the two-layer Oregon State University land scheme in CaRD10. The cloud schemes are based on the work of *Tiedtke* [1993] and are updated according to previous research by *Iacobellis and Somerville* [2000] and *Shimpo et al.* [2008]. These new physical processes are critical to regions in California. Nudging of the perturbation [*Yoshimura and Kanamitsu*,

2009; *Kanamitsu et al.*, 2010] is applied to prevent synoptic-scale drift. In this method, nudging is applied to the large-scale rotation part of the wind. The area-mean temperature is also nudged, but moisture is not nudged (see *Kanamitsu et al.* [2010] for further details).

2.2. Regional Ocean Modeling System (ROMS)

[12] The ROMS [*Shchepetkin and McWilliams*, 2005] is a free-surface, terrain-following, primitive equation ocean model. Initially, it was based on the S-coordinate Rutgers University Model (SCRUM) [*Song and Haidvogel*, 1994]. For computational economy, the hydrostatic primitive equations for momentum are solved using a split-explicit time stepping scheme, which requires special treatment and coupling between barotropic (fast) and baroclinic (slow) modes. In order to avoid errors associated with the aliasing of frequencies resolved by the barotropic steps, but unresolved by the baroclinic step, the barotropic fields are time-averaged before they replace values obtained with a longer baroclinic step. In addition, the separated time stepping is constrained so as to maintain exact volume conservation and consistency preservation properties that are needed for the tracer equations. In the vertical direction, the primitive equations are discretized over variable topography using stretched terrain-following coordinates.

[13] There are several subgrid-scale parameterizations in ROMS. The local closure schemes are based on level 2.5 turbulent kinetic energy equations [*Mellor and Yamada*, 1982] and generic length scale (GLS) parameterization [*Umlauf and Burchard*, 2003]. The nonlocal closure scheme is based on the K-profile, boundary layer formulation developed by *Large et al.* [1994]. The K-profile scheme has been expanded to include both surface and bottom oceanic boundary layers. In addition, there is a wave/current bed boundary layer scheme that includes bottom stress and sediment transport, which are important in coastal applications.

2.3. Coupling of RSM and ROMS

[14] The ROMS version 3.0 and the latest version of RSM are coupled in a parallel environment. The powerful and efficient MPI-2 method is used to couple the RSM and ROMS. Two independent executable jobs of RSM and ROMS run simultaneously, and the two models communicate at specific time intervals, e.g., 24 h. The RSM supplies atmospheric forcing to ROMS and in turn, receives SST data from ROMS. The atmospheric forcing from the RSM is directly utilized by ROMS, and ROMS offers SST data to the RSM without an SST-flux coupler. MATLAB was extensively used in the original ROMS preprocessing programs, which required intensive human interactions. All MATLAB programs have been converted to Fortran, and the human interaction processes have been completely eliminated in our system. These processes include automatic smoothing of coastal lines, smoothing the bathymetry, configuring the model vertical levels, and detecting open boundary positions.

[15] The regional ocean model typically suffers from large-scale error within the domain. This error is mostly caused by the systematic bias in the radiation fluxes reaching the sea surface. ROMS has a built-in correction scheme for radiation fluxes and fresh water fluxes so as to eliminate the development of large-scale error. In our previous experiments conducted with and without correction, it was found

that large-scale error in the SST develops within the domain if no corrections are applied. A systematic warm bias in uncorrected runs over the southern half of the domain was apparent. The error in the RSM forcing was found to be due to shortcomings in the total heat flux, mainly the incoming long and short wave radiation. Since significant effort is required to reduce inconsistencies in the RSM total heat flux, we tentatively decided to postpone our efforts in improving the RSM. Instead, we utilize the ROMS built-in heat flux correction scheme in the coupled integration experiments. The observed SST climatology and surface net heat flux sensitivity to the SST are provided externally in order to nudge the SST to its observed value [*Marchesiello et al.*, 2003]. This bias correlation may also depress the development of the surface ocean state.

2.4. Experimental Design

[16] An uncoupled experiment, forced by the prescribed SST, was conducted as a control run (hereafter called the UNCPL experiment); the RSM configurations in the experiment followed *Miller et al.* [2009]. Another experiment with the coupled model (hereafter known as the CPL experiment) described above was also carried out.

[17] The RSM and ROMS share the same domain with a 10-km resolution in the CPL experiment. The model domain covers the California Current System (CCS), which is a complicated eastern boundary current. The CCS consists of the large-scale California Current, Davidson Current, California Undercurrent, and the Southern California Eddy [*Hickey*, 1998]. The fine-scale coastal features of upwelling fronts, mesoscale and sub-mesoscale eddies, and meanders are also included. The domain (Figure 1) covers the area from 19.558°N to 50.22°N and 135.26°W to 103.58°W. This model domain is much larger than the CaRD10 domain (29.466°–45.719°N, 128.203°–111.563°W) and thus, the California Current System and the southwestern monsoon over the Gulf of California are included in the domain. Three sub-domains, A, B, and C, are employed in the study. The largest sub-domain, A, is used to examine the large-scale pattern of the ocean surface current and SST. The upwelling cold tongue region is included in the middle sub-domain, B, which is used to study the impact of upwelling on the atmosphere. The smallest sub-domain, C, is located at the Southern California Bight, which is where the local Catalina Eddy mesoscale circulation develops.

[18] The RSM is in 28 vertical atmosphere sigma levels, while ROMS is in 30 vertical ocean sigma levels. The atmospheric lateral forcing for the UNCPL and CPL experiments is the T62L28 6-hourly NCEP/DOE reanalysis (R-2) [*Kanamitsu et al.*, 2002]. The SST for the UNCPL run is from the NCEP weekly analysis [*Reynolds and Smith*, 1994]; it is interpolated to the daily analysis data using mean conserving interpolation [*Taylor et al.*, 2000]. One may argue that the satellite retrieved high-resolution daily SST can be used in the UNCPL run. We selected this SST since the data have been thoroughly checked in several reanalysis projects and were readily available. The resolution of these data is one degree and will hereafter be called the NCEP SST. The Monthly Simplified Ocean Data Assimilation (SODA) [*Carton et al.*, 2000] was used for the ROMS oceanic initial and boundary conditions in the CPL downscaling. The horizontal resolution of SODA is 0.5 degrees in
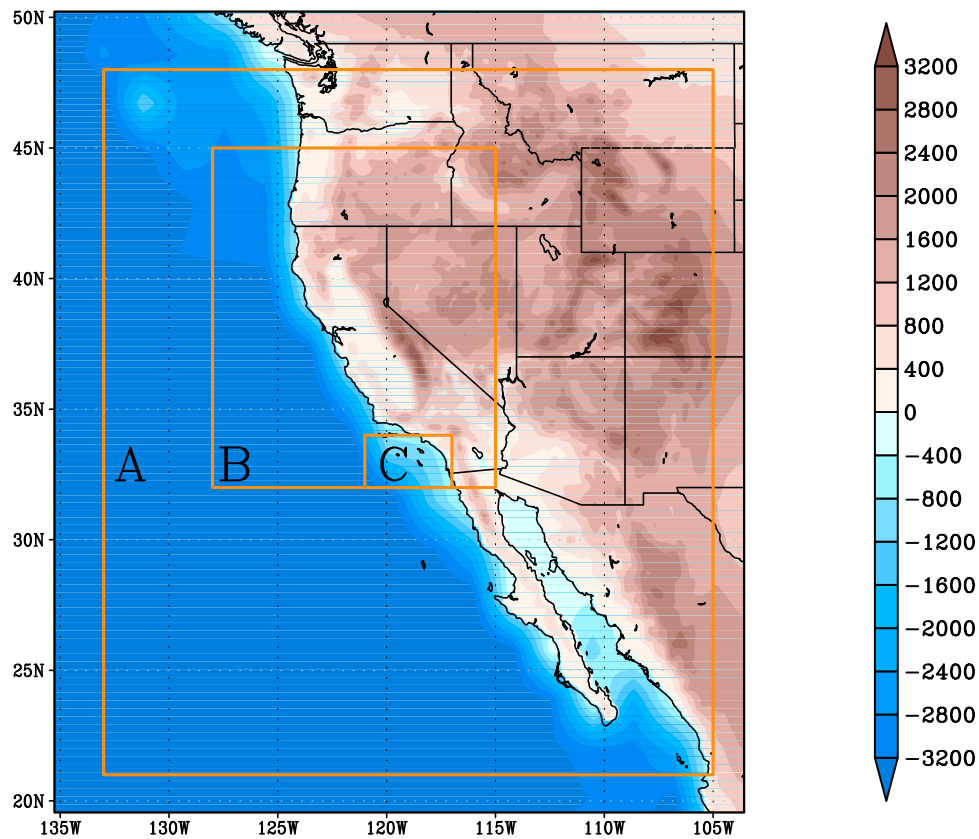
Figure 1. Model domain, RSM elevation (m), and ROMS bathymetry (m). Domain A is used to examine the large-scale pattern of the ocean surface current and SST, while the upwelling impact to California is examined in the middle domain, B. The smallest domain, C, is used to study the Catalina Eddy.

30 vertical levels. RSM uses the ROMS SST field in the CPL experiment. Since the NCEP SST is available on a daily time scale, a 24-h communication interval is employed in the CPL run. The instant SST at the end of a 24-h integration period is sent to the atmosphere part of the model and is also used for verification. The monthly mean NCEP SST and heat flux sensitivity computed from the UNCPL run is used in the ROMS built-in correction [*Marchesiello et al.*, 2003] scheme so as to avoid the large-scale SST bias in the CPL experiment.

[19] The spin-up time here is on the order of two years, which is the same as that noted by *Marchesiello et al.* [2003] in their climatological experiments. The twelve-year integration period (1994–2005) is the same for both the CPL and UNCPL experiments. The first two years of the CPL run is for spin-up, while the remaining 10 years are used for analysis. The atmospheric variables from the CPL and UNCPL experiments are saved every hour, and the oceanic fields of the CPL are saved every 24 h.

3. Oceanic State

[20] Only the ocean surface current and SST features are presented in this work. A detailed analysis of the 3D ocean state from the CPL experiment will be presented in a future paper. The summer upwelling is the dominant phenomenon over the California Current System, and it results in distinct differences in the atmospheric states in the CPL and UNCPL experiments.

3.1. Ocean Surface Current

[21] The ocean surface current climatology from the SODA and CPL run is shown in Figure 2. In the summer, upwelling is prevalent along the California coast due to winds along the shore (Figures 2a and 2b). In the winter, the widely equatorward large scale California Current is located offshore in SODA (Figure 2c) and the CPL experiment (Figure 2d). A strong recurring poleward current is also observed along the coast of Oregon in SODA and the CPL run; this current is related to the surface wind direction. It is apparent that the surface coastal currents are stronger in the summer than in the winter. In the CPL experiment, the large-scale current patterns were similar to those in SODA, but with smaller scale features. For example, the CPL results show distinct anti-cyclonic small eddies offshore of Los Angeles, and a stronger cyclonic eddy near the western boundary between 30°N and 35°N (Figures 2c and 2d). The enhanced mesoscale eddy features in the CPL experiment are in part due to the difference in the horizontal resolution (10-km for the CPL run versus 0.5° for the SODA reanalysis). It was also found that the CPL simulated coastal current (Figure 2b) is stronger than the SODA coastal current (Figure 2a).
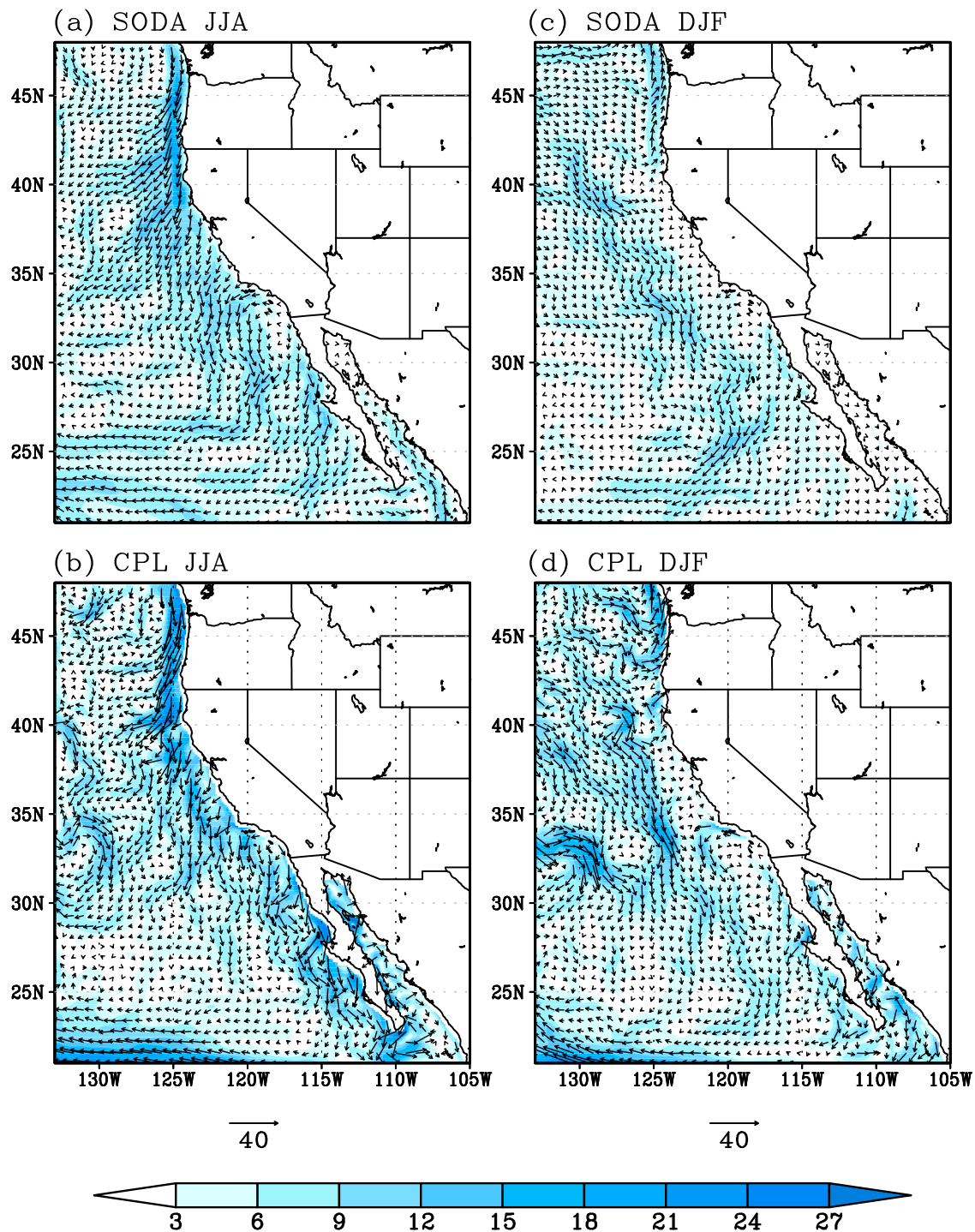
Figure 2. Summer seasonal climatology surface current (cm/s) from (a) SODA and (b) the CPL run, and the winter seasonal climatology surface current from (c) SODA and (d) the CPL run.

3.2. Sea Surface Temperature (SST)

3.2.1. Seasonal Climatology

[22] The resolution for the SST is 10-km and one degree for the CPL simulation and NCEP observations, respectively. The SST from the Advanced Very High Resolution Radiometer (AVHRR) Pathfinder V5 (ftp://podaac-ftp.jpl.nasa.gov/allData/avhrr/L3/pathfinder_v5/monthly/) with 4-km resolution was employed to evaluate the performance of the

CPL-simulated SST. The 10-year (1996–2005) summer climatology from the 4-km AVHRR, one-degree NCEP, and CPL-simulated SST are shown in Figure 3. Generally speaking, the large-scale pattern of the CPL-simulated SST agrees very well with the AVHRR and NCEP results. The 18°C cold tongue of these three SSTs is located at the Southern California Bight (Figures 3a–3c). In addition, the CPL SST was found to be colder than that from AVHRR and NCEP observations along the California coast. The difference
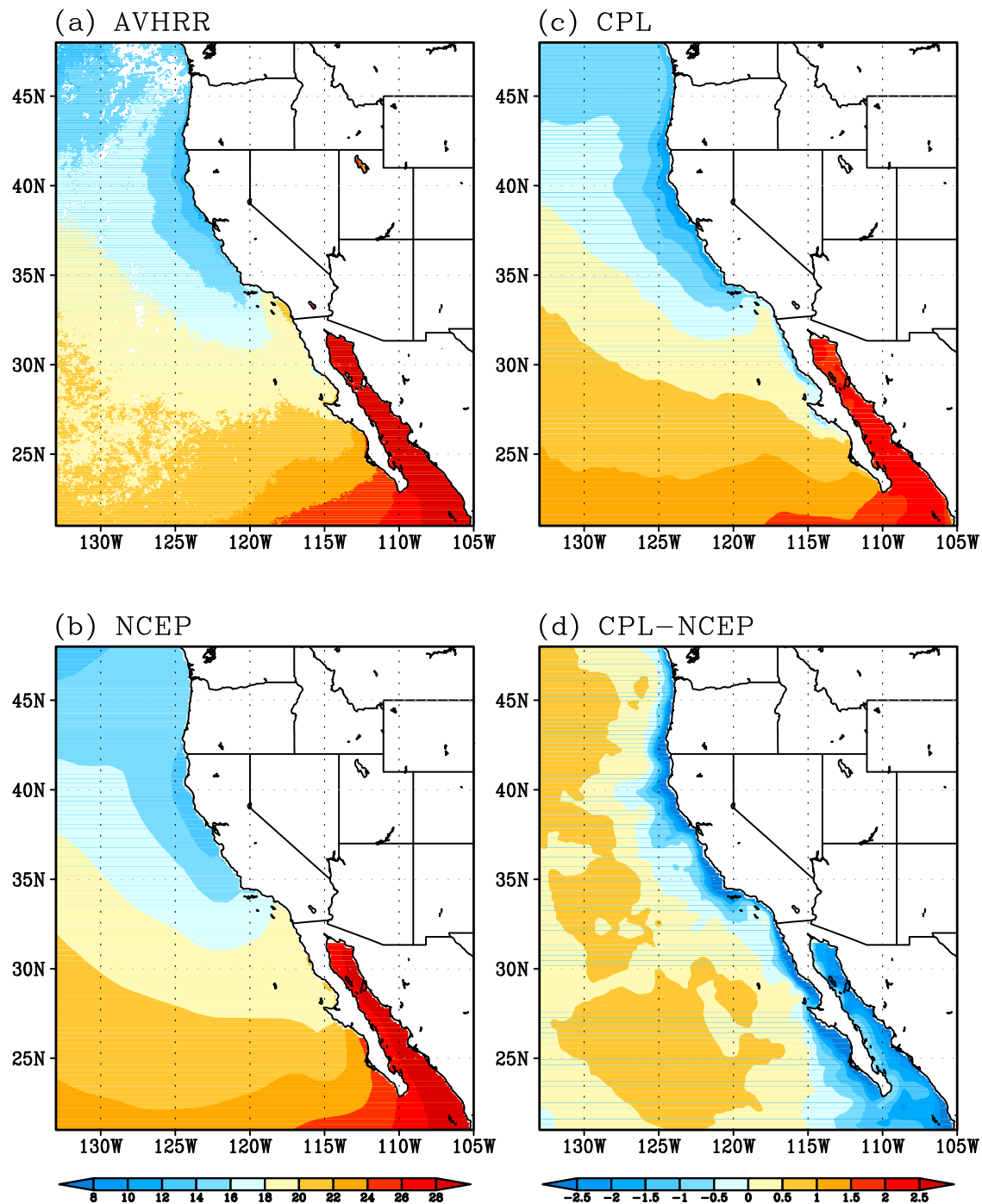
Figure 3. Summer SST climatology (°C) from (a) the AVHRR, (b) NCEP, and (c) the CPL run, and (d) the difference between the NCEP and CPL runs.

between the CPL and NCEP SST in the winter was not as significant as in the summer. However, the winter CPL SST is about 0.5~1°C colder around Southern California when compared to the SST from NCEP and AVHRR observations (not shown).

[23] The summer SST difference between the CPL run and NCEP is displayed in Figure 3d. There is a narrow belt of cold SST difference along the coast that has a strong intensity. It is noted that the cold belt is narrowest over the Bight of Southern California, which is a region of weak

winds. The warm SST difference near the western boundary and over the Southern Ocean domain should be caused by the surplus net heat flux in the coupled model, although the net heat flux correction was applied in the ocean model.

3.2.2. Monthly Mean SST

[24] The monthly mean SST in the upwelling season (May through September) should also be examined, as these small-scale features would be smoothed out in climatology. August 2005 was arbitrarily selected from the long-term CPL run. The upwelling cold tongue of the AVHRR, NCEP,
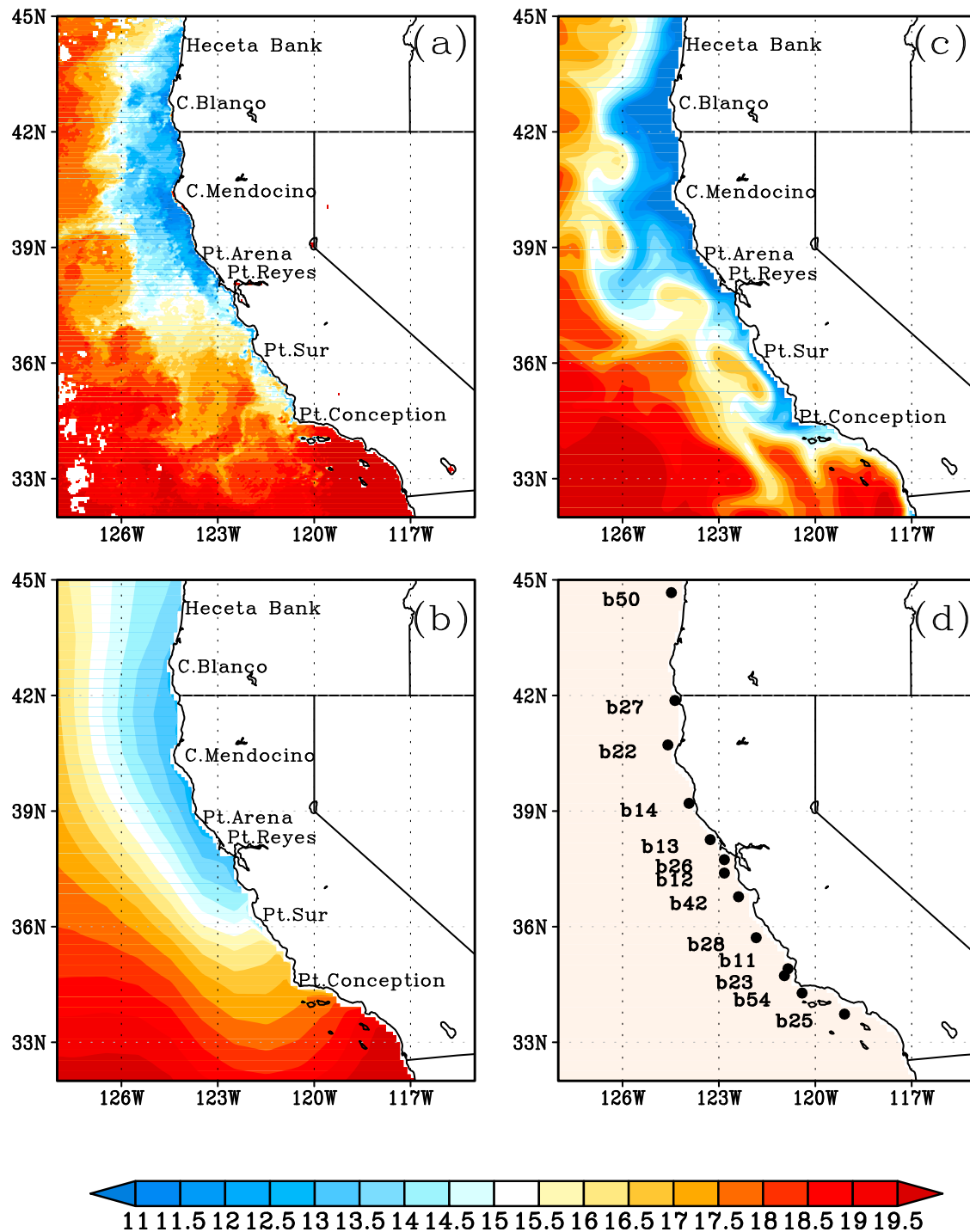
Figure 4. August 2005 monthly mean SST (°C) from (a) the 4-km AVHRR, (b) NCEP, and (c) the CPL run. (d) The distribution of buoy stations.

and CPL simulated SST in this month is shown in Figure 4. There are many mesoscale variability patterns in the 4-km AVHRR SST (Figure 4a). The upwelling cold tongue resides between Heceta Bank and Point Reyes, and the colder SST propagates from Cape Blanco, Cape Mendocino, and Point Arena. The cool offshore filaments extend from Point Sur and Point Conception. The upwelling cold tongue of the NCEP SST is very weak and smooth; mesoscale features are not apparent in the one-degree NCEP SST

(Figure 4b). In contrast, all of these mesoscale SST features are captured in the physically resolved 10-km CPL simulated SST (Figure 4c), and the finer patterns of the CPL-simulated SST are comparable to those of the 4-km AVHRR SST. It is also apparent that along the coast from Heceta Bank to Point Conception, the NCEP SST is warmer than the AVHRR SST, but the CPL SST is colder than the AVHRR SST.

Table 1. The Daily SST Bias (°C) and RMSE (°C) of the CPL and NCEP SST Against Buoy Observations in July (January) of Each Year

	Bias		RMSE	
	NCEP	CPL	NCEP	CPL
1996	0.82 (0.26)	−1.69 (−1.07)	1.51 (0.67)	2.32 (1.21)
1997	1.14 (0.17)	−0.82 (−1.29)	1.44 (0.50)	1.75 (1.49)
1998	0.56 (−0.03)	−2.59 (−1.36)	1.33 (0.39)	2.88 (1.39)
1999	1.08 (0.15)	−1.55 (−0.71)	1.63 (0.53)	1.99 (0.84)
2000	1.12 (0.19)	−1.52 (0.24)	1.71 (0.45)	2.05 (0.54)
2001	0.74 (0.04)	−2.06 (−1.00)	1.41 (0.32)	2.40 (1.07)
2002	0.83 (0.07)	−1.00 (0.14)	1.67 (0.48)	1.85 (0.52)
2003	0.97 (−0.06)	−1.71 (−0.21)	2.16 (0.45)	2.41 (0.53)
2004	0.53 (0.06)	−1.95 (−0.82)	1.52 (0.48)	2.41 (0.92)
2005	0.73 (1.09)	−2.45 (−0.19)	1.48 (1.71)	2.91 (1.34)
Average	0.85 (0.19)	−1.73 (−0.49)	1.59 (0.60)	2.23 (0.99)

3.2.3. Validation Against Buoy Observations

[25] The daily variation in the CPL simulated SST is validated by National Data Buoy Center (http://www.ndbc.noaa.gov/) buoy observations and compared with the NCEP SST used for the uncoupled downscaling. The locations of the buoy stations (station names start from "b") are displayed in Figure 4d. There are thirteen coastal buoy stations with the Oregon coast (Stonewall Banks, b50) to the South California Bight (Santa Monica Basin, b25). The daily buoy SST was averaged from hourly observations, as the coupling interval is 24 h.

[26] The daily SST bias and root mean square error (RMSE) of the CPL and NCEP SST against the buoy observations in each July of the 10 analyzed years are shown in Table 1. The NCEP SST was found to have a warm bias of 0.85°C, while the CPL SST has a cold bias of −1.73°C. The RMSE in July is 1.59°C and 2.23°C for the NCEP and CPL SST, respectively. The bias and RMSE in January are given in brackets in Table 1. The bias in January for the NCEP SST is 0.19°C, while it is −0.49°C for the CPL SST. The RMSE for the NCEP and CPL SST is 0.60°C and 0.99°C, respectively.

[27] The variances from the buoy observations, CPL run, and NCEP run were computed at the buoy stations. The temporal correlation of the two analyses from the CPL and NCEP SST against the buoy observations was also calculated. The correlations and standardized deviations are shown in a Taylor diagram in Figure 5. In July, it is seen that all of the variance from the CPL run is greater than that from the buoy observations, while the corresponding NCEP value is much smaller than that from the buoy observations (Figure 5a). On average, the variance from the CPL run is 42.7% higher than that from the buoy observations, whereas the value from the NCEP SST is 54.5% smaller.

[28] Overall the correlation from the CPL SST is greater than that from the NCEP SST (Figure 5a). For example, in July 2000, there are 11 stations of the CPL temporal correlation that pass the 95% level of Fisher's exact significant test, while only 5 stations of the NCEP SST temporal correlation pass the significant test. The average correlation coefficient from the CPL and NCEP SST is 0.50 and 0.36, respectively. The correlation and variance scores in January from the NCEP and CPL SST are shown in Figure 5b. The computed variance from the CPL run is about 87% closer to

the observed values when compared to the NCEP SST, although the correlation coefficients are similar.

[29] The improvement in the temporal correlation by the CPL simulated SST is quite significant in the summer, but not readily apparent in the winter. The coastal SST is less active in the winter than in the summer, since the buoy observation variance is much smaller in the winter. This phenomenon is captured by the CPL simulated SST, but is not reflected in the NCEP SST. The one-degree NCEP daily SST is interpolated from the weekly SST, while the CPL daily SST is physically resolved from the ocean model in 10-km high resolution. It is concluded that the daily coastal
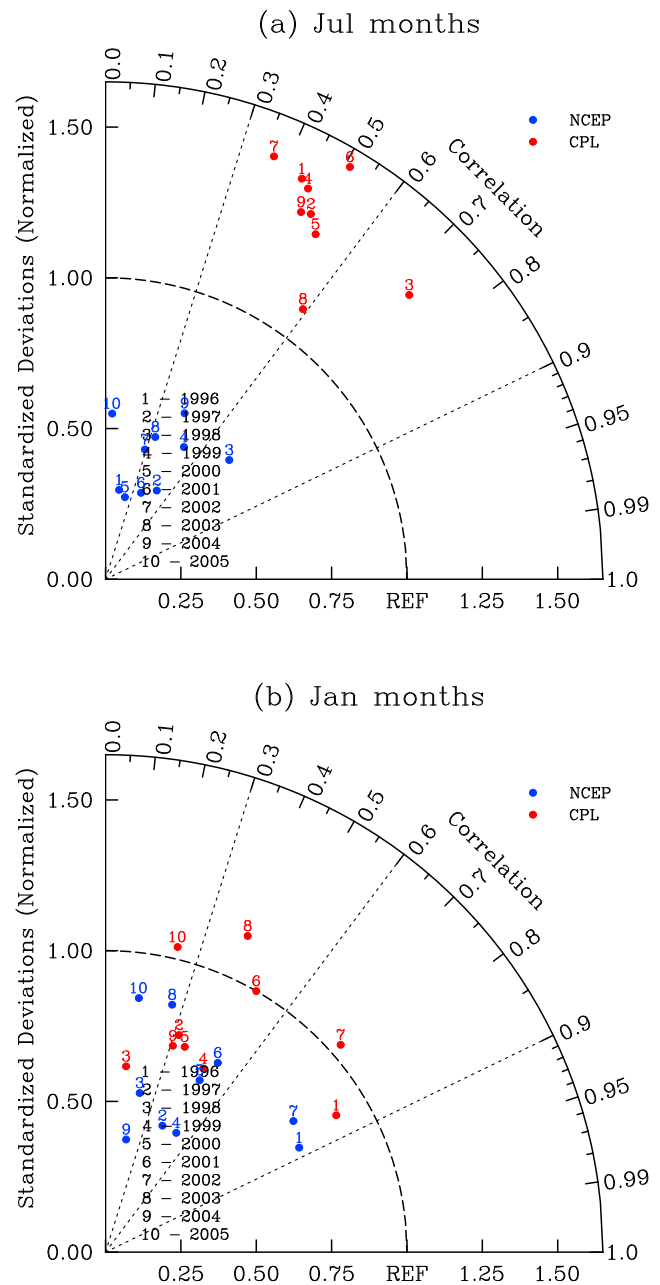

Figure 5. Taylor diagrams of NCEP and CPL daily SST against buoy observations in (a) July and (b) January of each year.
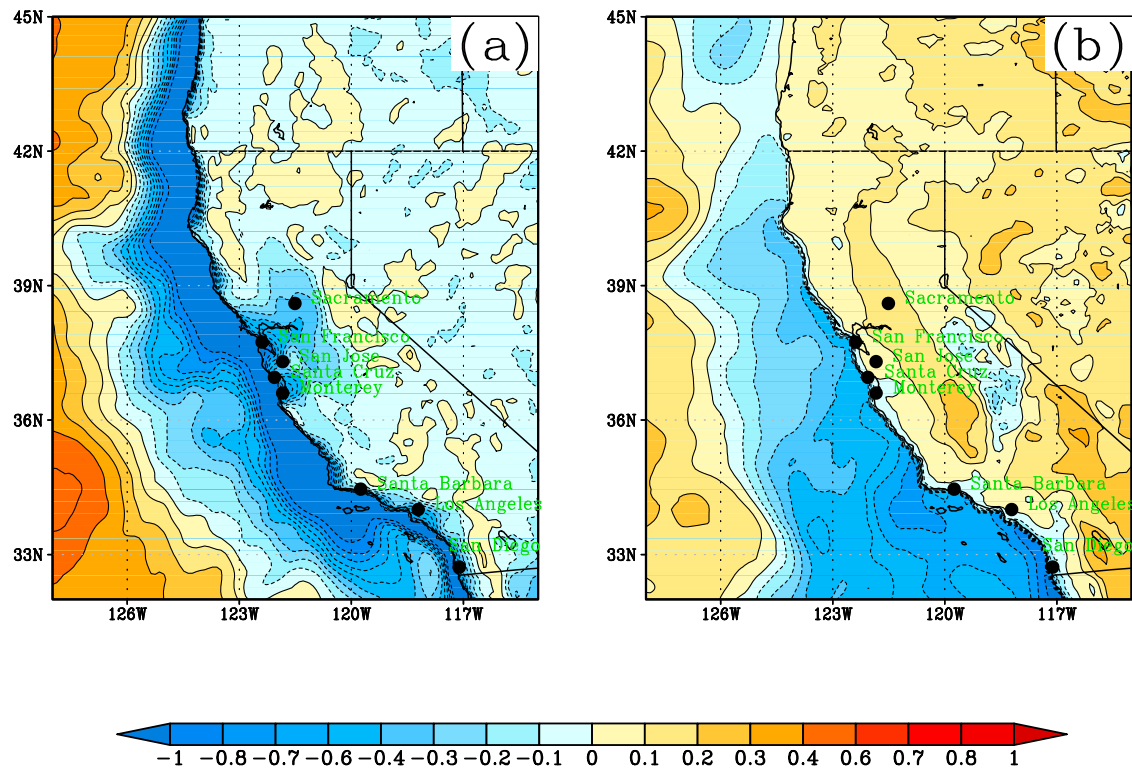
Figure 6. Difference in the T2m climatology (°C) of the CPL and UNCPL runs in (a) summer and (b) winter.

simulated SST in the coupled model is more realistic than the NCEP daily SST in the upwelling season.

4. Atmospheric Climatology

[30] Differences in the atmospheric climatology from the CPL and UNCPL runs are discussed in this section. Particular focus is placed on the regions over California and the nearby coastal areas. Due to a dry season over California in the summer, the difference in precipitation for the CPL and UNCPL experiments is not significant. Therefore, the surface air temperature, surface wind, cloud cover, and planetary boundary are emphasized.

4.1. Surface Air Temperature

[31] The difference in the surface air temperature (T2m) climatology for the CPL and UNCPL experiments in the summer and winter is shown in Figure 6. The T2m difference pattern over the ocean matches the SST difference pattern due to boundary layer vertical mixing. In the winter, there is only a very narrow and weak cooling difference band over land along the coastline of Central and Southern California (Figure 6b). In the summer, the cooling difference area over coastal land is much wider and stronger than in the winter (Figure 6a). The cooling difference is apparent over the entire Central Valley. This corresponds to the complex topography along the California coast (Figure 1). The coastal mountain range runs from north of Del Norte County to south of the Mexican border, with a break at the Golden Gate. The surface air-cooling difference is influenced by dramatic changes in elevation. The mountain blocking effect

is weak at the location of the break, and the advection transport of coastal cool air to the inland region is far.

[32] In order to quantitatively detect the T2m difference over the coastal areas, six cities along the California coast and two inland cities over the San Francisco Bay (San Jose and Sacramento) are marked in Figure 6. In the winter, the temperature difference over these cities is very small. The biggest difference is evident over the city of San Diego, which is cooled by 0.31°C. Of all the seasons, the cooling differences are strongest over all eight cities in the summer, particularly over the San Francisco Bay area. The coastal city of San Francisco is cooled by 1.11°C, and even the inland cities of San Jose and Sacramento are cooled by 0.38°C and 0.34°C, respectively.

[33] The surface air temperature bias from the CPL and UNCPL runs are examined against Cooperative Observer Program (COOP, http://www.nws.noaa.gov/os/coop/) station data. The annual cycle of T2m bias over San Francisco, Santa Cruz, and Los Angeles is plotted in Figure 7. Due to a cooling effect along the coast in the summer, the intraseasonal variability is reduced in the CPL run. The UNCPL run shows a warm bias of 0.39°C in the summer over San Francisco, while the CPL run exhibits a cold bias of −0.72°C. Over Santa Cruz, the UNCPL run shows warming by about 1.92°C in the summer, which is reduced to 1.43°C by coupling. The UNCPL run has a warm bias of 0.24°C in the summer over Los Angeles, while the CPL experiment has a cold bias of −0.44°C. The UNCPL run tends to have a cold bias in the non-upwelling season, but a warm bias in the upwelling season. The difference in the monthly T2m bias difference for the CPL and UNCPL runs is very small in the
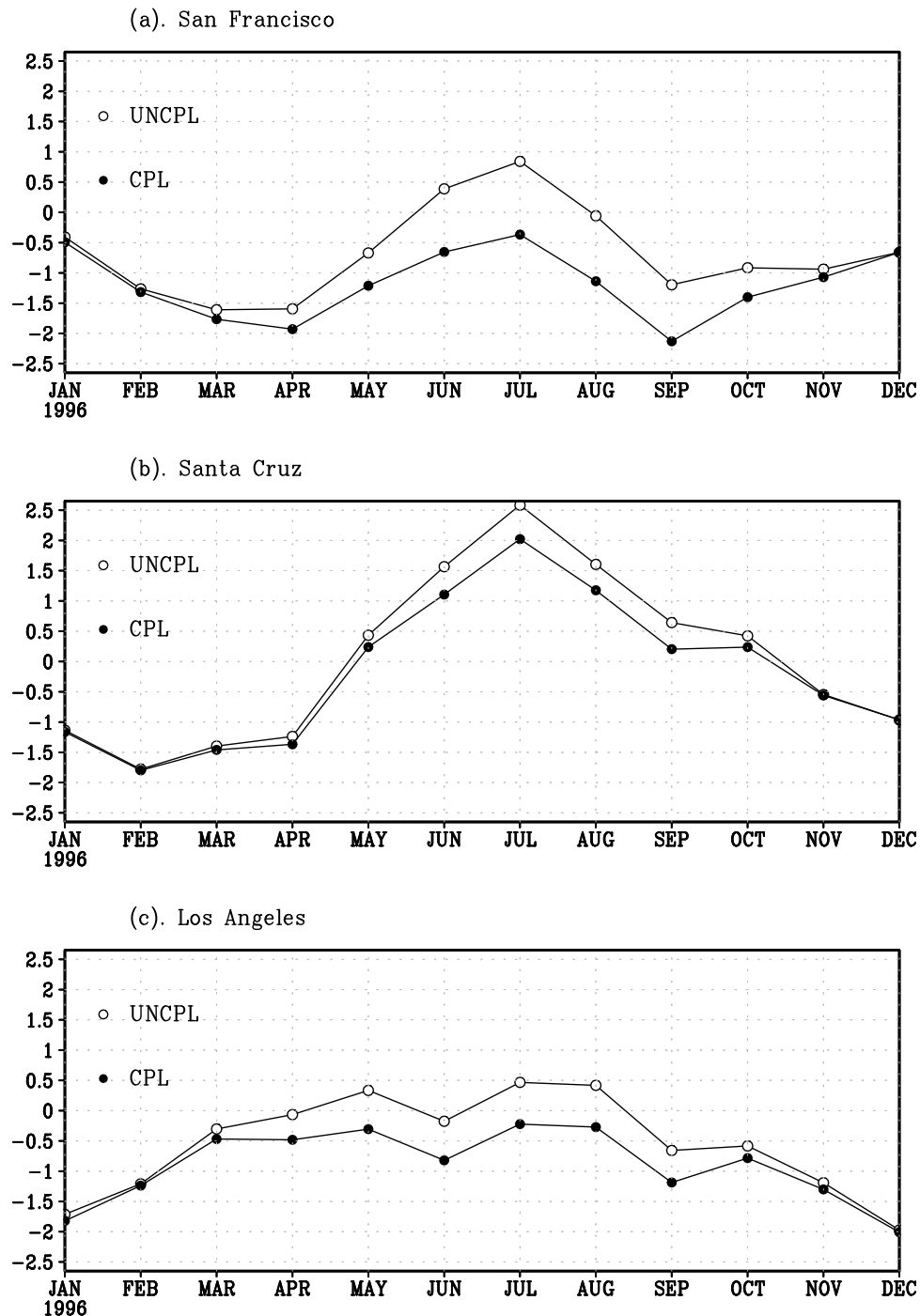
Figure 7. T2m monthly climatology (1996–2005) bias (°C) of the CPL and UNCPL runs against COOP observations over (a) San Francisco, (b) Santa Cruz, and (c) Los Angeles.

winter and becomes larger from May to September (upwelling season).

[34] The onshore wind and temperature gradients contribute to cold temperature transport from ocean to land. The larger land-sea temperature contrast in the CPL experiment may increase the extent of land-sea breeze, which will in turn influence the air temperature. Land-sea breeze is more thoroughly analyzed in part b) of Section 5. Unfortunately, the sea breeze difference for the CPL and UNCPL runs is too small to have any statistically significant meaning. Thus, the temperature gradient plays a more important role than sea breeze in surface air temperature variations.

4.2. Surface Winds

[35] The large-scale wind patterns from the CPL and UNCPL runs are quite similar. The wind is much stronger in the summer than in the winter. The equatorward wind along the shore is dominant with a maximum speed greater than 7 m/s along the coast of California. However, this wind has a speed of less than 5 m/s near the coast of the Southern
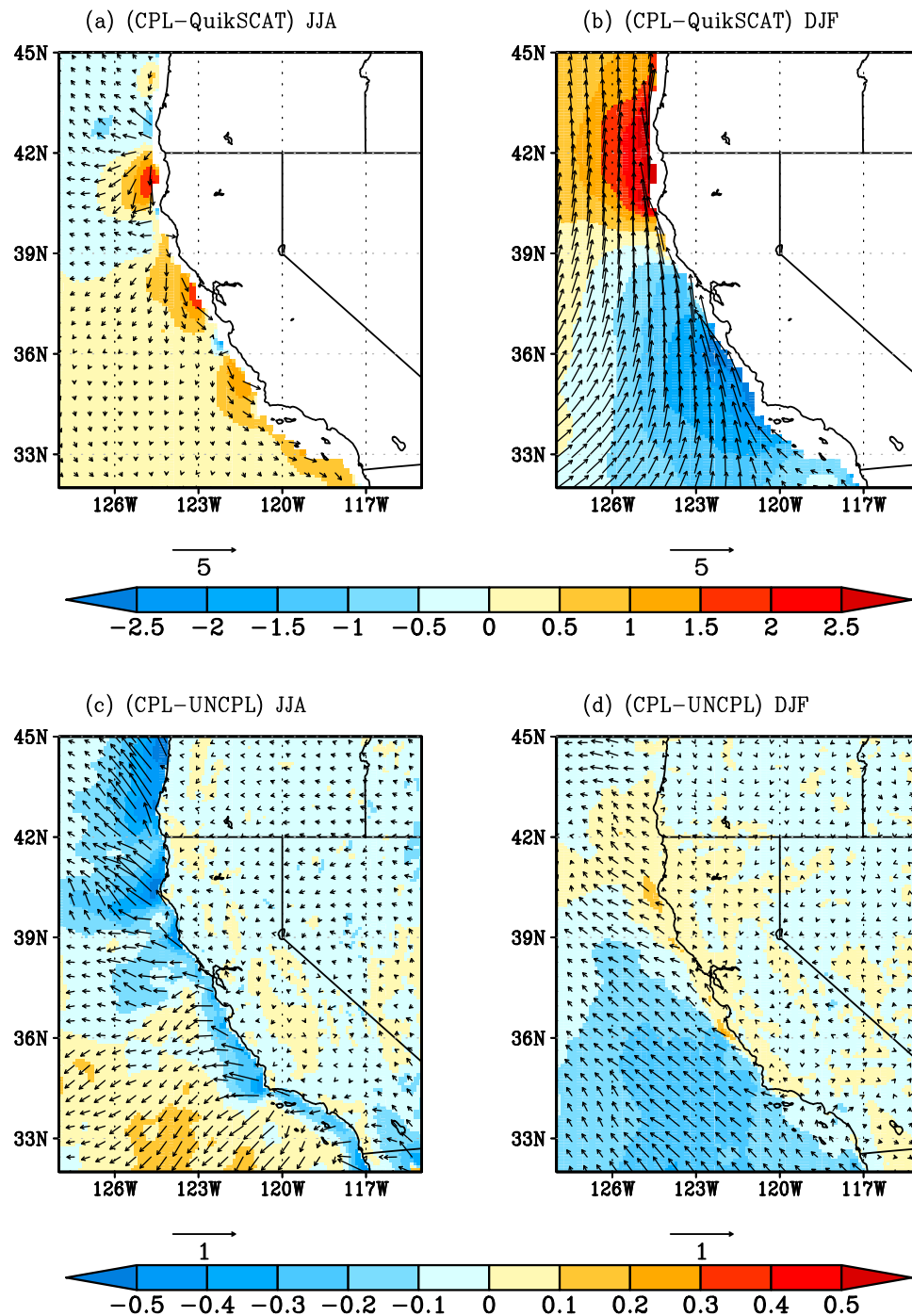
Figure 8. Difference in the 10-m wind climatology (m/s) of the CPL run and QuikSCAT in (a) summer and (b) winter; 10-m wind climatology difference (m/s) between the CPL and UNCPL runs in (c) summer and (d) winter.

California Bight. In the winter, the westerly wind blows from the Pacific Ocean and separates into northward and southward branches at the coast of Central California. The mean wind speed is about 1–2 m/s around the coastal area of Central California and the Bight of Southern California, and reaches about 3–4 m/s over the coast of Oregon and 100 km offshore of the Southern California Bight.

[36] The wind climatology from the CPL and UNCPL experiments is compared with Oregon State University QuikSCAT observations (http://cioss.coas.oregonstate.edu/scow/). The QuikSCAT climatology data are from 1999 to 2009, whereas the model climatology data are from 1996 to 2005. In the summer, the CPL wind speed is stronger than that from QuikSCAT observations along the coast of California (Figure 8a). This may in turn result in stronger upwelling. In the winter, the CPL wind speed was found to be stronger than that from observations over the coast of North California and weaker over the coast of Central and

Southern California (Figure 8b). The southwesterly wind difference will induce the southeastward transfer of cold water, which may result in a cold bias over the Southern California coast.

[37] The wind vector and wind speed differences between the CPL and UNCPL experiments in the summer and winter are shown in Figures 8c and 8d, respectively. Coastal northwestward wind vector differences are evident in each season. In the summer, the wind speed from the CPL experiment is reduced along the coastal ocean region, but the difference is very small over land (Figure 8c). In the winter, the coastal wind speed from the CPL run is enhanced between Point Sur and Cape Mendocino (Figure 8d). The wind speed over the offshore region between Point Conception and Point Sur is reduced by as much as 15%. The wind speed is also reduced between San Diego and Los Angeles. The difference in the surface air temperature for the CPL and UNCPL runs leads to a surface pressure difference, which further induces a wind difference. The surface wind may also increase (decrease) over warm (cold) water in association with a decrease (increase) in the stability of the boundary layer [*Chelton and Xie*, 2010]. We further compared the CaRD10 wind climatology with the QuikSCAT climatology over the same period of 1999–2009. The CaRD10 summer wind is also stronger than the QuikSCAT wind (not shown). It is concluded that the summer coastal wind from the UNCPL experiment is partially improved by air-sea interactions.

4.3. Cloud Cover

[38] The difference in the upper atmosphere for the CPL and UNCPL runs was studied by examining cloud cover and boundary layer height. Low clouds are usually situated from the near surface up to an altitude of 2000 m, while middle clouds are formed at 2000 m or even higher altitudes in some regions. High clouds can be formed at altitudes between 5000 and 12000 m in the temperate regions. The simulated high, middle, low, and total cloud amounts were calculated using a maximum-random overlap assumption [*Chou et al.*, 1998].

[39] In the winter, the difference in the low cloud, middle cloud, and high cloud cover in the CPL and UNCPL runs is very small (not shown). In the summer, low cloud cover from the CPL run is reduced over most areas of California. Specifically, low cloud cover is reduced by more than 10% over land between Point Conception and Point Sur, and over the ocean near Catalina Island (Figure 9a). Middle cloud cover from the CPL experiment is reduced over the ocean south of Point Sur, and enhanced over the ocean north of Point Sur (Figure 9b). The difference in high cloud cover for the CPL and UNCPL runs is small, and there are only a few spots with a difference of over 3% (Figure 9c). The surface temperature from the CPL experiment is cooler than that from the UNCPL run during the summer, which makes evaporation a little weak and reduces the humidity. The cold coastal SST in the CPL run should enhance low-level atmosphere inversion and help to form more low-level marine layer clouds, which are prevalent over the California coastal areas. This is different from the scenario of reduced cloud cover in Figure 9a. Such an opposite relation may be due to the strong dependency of the computed cloudiness on the relative humidity in the cloud scheme [*Shimpo et al.*, 2008].

A relatively coarse vertical resolution for representing the temperature inversion can be another factor. The difference in cloud cover in the CPL and UNCPL runs is strong in the low troposphere, but weak in the upper troposphere.

4.4. Planetary Boundary Layer Height

[40] The planetary boundary layer height (PBLH) is lower along the California coast than over the nearby ocean and continent. The lowest PLBH is found over the Southern California Bight; it is about 400–500 m in the winter and only 200–300 m in the summer (not shown). The difference in the PBLH for the CPL and UNCPL runs in the summer is shown in Figure 9d. The PBLH of the CPL run is reduced by as much as 15% along the coastal ocean area. It is also apparently reduced by more than 3% over the San Francisco Bay area, where the surface air temperature is much cooler than in the other land areas. The cooler surface temperature between the CPL and UNCPL runs increases the stability of the boundary layer.

5. Mesoscale Impact Study

5.1. Catalina Eddy

[41] The Catalina Eddy (CE) is a type of localized weather phenomenon along the coast of Southern California. The CE develops when the regular northwesterly flow changes direction and turns to southerly flow along the California coast, producing a mesoscale cyclonic circulation over the Southern California Bight.

[42] In this study, CE events are defined as near-surface cyclonic circulation localized within the Bight of Southern California and centered near Santa Catalina Island. A composite of the wind field 10 m above the surface was used for CE event detection. The same composite 10-m wind map of the canonical eddy and method are applied to detect CE cases in the CPL and UNCPL experiments. The spatial pattern correlation between the composite near surface wind directions and the hourly CPL and UNCPL 10-m wind directions are then calculated within the rectangular area 32°N–34°N, 121°W–117°W. The Pearson product-moment correlation coefficient is used here since we are only interested in the wind direction and not the amplitude. It was assumed that a CE occurred if the correlation coefficient was larger than a certain threshold of 0.7, which represents significant cyclonic rotation over the Bight of Southern California.

[43] The detected Catalina Eddy hours from the CPL and UNCPL experiments during the 10 analyzed years (1996–2005) are listed in Table 2. A total of 2574 CE hours are detected in the UNCPL run, while 2742 CE hours are detected in the CPL experiment. The CPL run tends to generate 6.5% more CE hours than the UNCPL run. The increase in CE events is observed for durations of 1–2 h and 7–8 h (Table 2). The 10-year Catalina Eddy hours were composited to one map for the CPL and UNCPL experiments (Figure 10). It is clearly seen that the cold SST along the coast is located toward the eastern edge of the CPL composite Catalina Eddy. *Ulrickson et al.* [1995] noted this cold tongue formation along the coast in their numerical simulation. A warm anomaly along the west of the CE and a cold anomaly along the eastern edge of the eddy during the CE full development stage were also found from CaRD10.
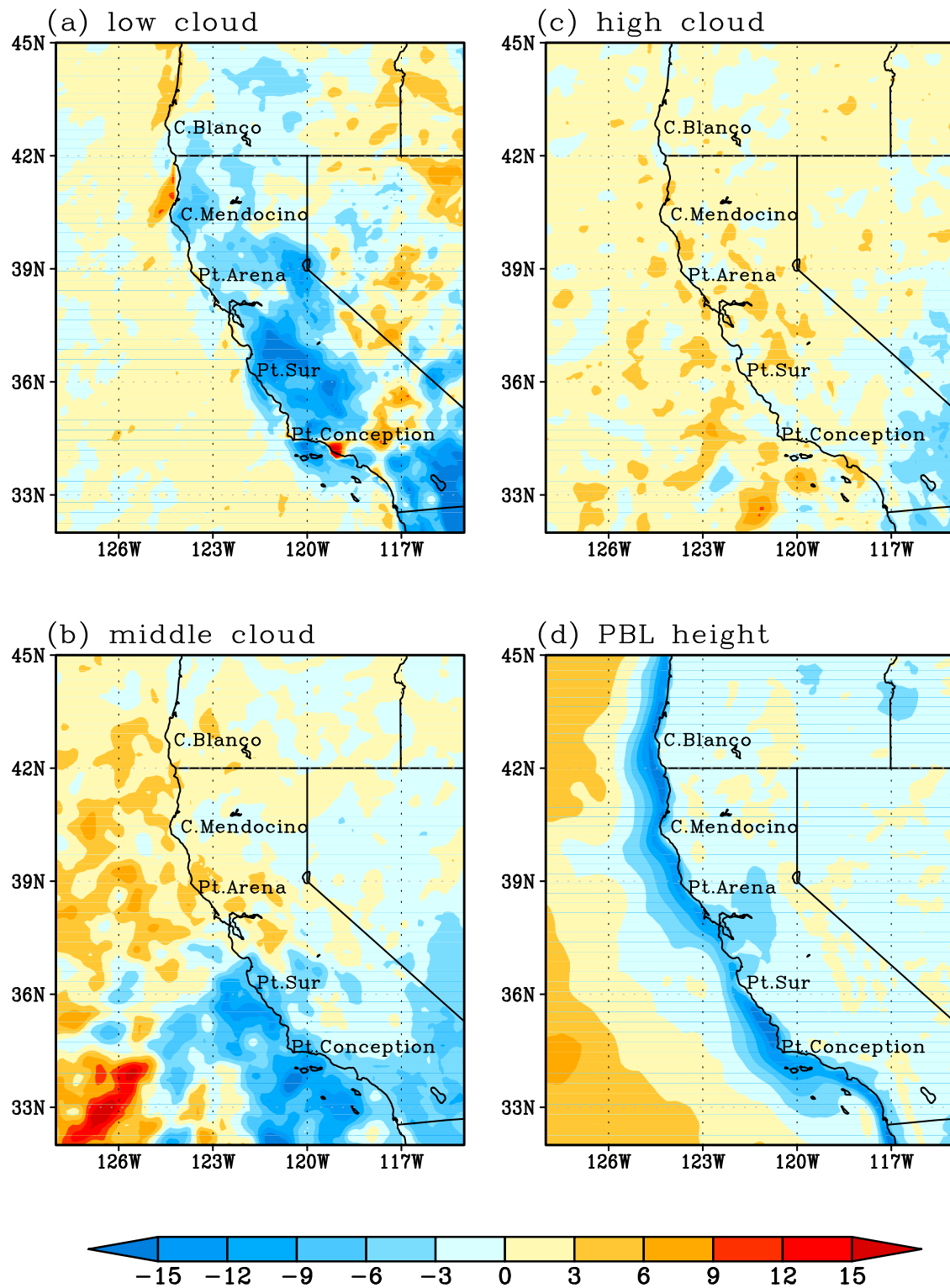
Figure 9. Difference in the relative summer climatology (percentage) of (a) low cloud cover, (b) middle cloud cover, (c) high cloud cover, and (d) planetary boundary layer height from the CPL and UNCPL runs.

It is believed that the cold SST along the coast in the CPL run enhances the development of the Catalina Eddy.

5.2. Land Sea Breeze

[44] Over the coastal areas, the temperature difference between land and sea will modulate the pressure gradient in the lower troposphere, which can in turn affect low-level sea breeze circulations during the day and land breeze at night.

[45] The hourly climatology winds above 10 m during the summer from the CPL and UNCPL experiments are used to analyze the land-sea breeze. Onshore and offshore winds perpendicular to the coastal line are decomposed from the

Table 2. The Number of Detected Catalina Eddy Hours and the Duration (Hours) of Catalina Eddy Events in the UNCPL and CPL Runs

Year	CE Hours			CE Events Duration		
	UNCPL	CPL	Overlap	Duration	UNCPL	CPL
1996	219	245	164	1	252	234
1997	232	276	176	2	156	197
1998	157	191	109	3	131	122
1999	265	282	195	4	88	83
2000	293	315	201	5	67	66
2001	206	213	144	6	39	35
2002	353	354	253	7	28	42
2003	308	322	216	8	18	19
2004	235	232	155	9	10	12
2005	306	312	213	Over 10	20	18
Total	2574	2742	1826	Total	809	828

zonal and meridional winds. The difference in the onshore sea breeze for the CPL and UNCPL runs were evaluated by a Student's *t*-test in order to examine the statistical significance over the time period of 11 A.M.–4 P.M. PT. The difference in the offshore land breeze for the CPL and UNCPL runs was also evaluated by a Student's *t*-test over the time period of 11 P.M.–4 A.M. PT. The onshore sea breeze difference between the CPL and UNCPL experiments is too small to have a statistically significant meaning (not shown). This is likely due to the 24-h coupling interval in the CPL run, which is the same as that used to obtain the daily NCEP SST. In contrast, the difference in the land breeze for

the CPL and UNCPL runs is statistically significant and enhanced by as much as 10%. There is a negative offshore surface air temperature difference gradient between the CPL and UNCPL (Figure 6b) experiments that causes an offshore positive pressure difference gradient. This in turn enhances the intensity of the land breeze by coupling.

6. Conclusions

[46] A fully regional ocean atmosphere coupled modeling system was developed at the Scripps Institution of Oceanography (SIO). Twelve-year reanalysis coupled downscaling was performed over the western North American continent and the nearby ocean. Specifically, the analyzed region was centered at California. The ocean and atmosphere models share the same domain and 10-km resolution grid. The SST and atmospheric-flux coupling interval was 24 h. The first two years were used for ocean spin-up purposes, while the remaining ten years were employed for the analysis.

[47] The large scale pattern of the ocean surface current in the SODA oceanic reanalysis is reserved by coupled downscaling, and more fine-scale oceanic features are generated with the high-resolution ocean model. The simulated SST was compared and validated with the one-degree NCEP SST, 4-km AVHRR satellite SST, and buoy observations over different time scales. The seasonal climatology SST pattern from the CPL experiment is in good agreement with the AVHRR and NCEP SST. The simulated SST is lower than the NCEP SST along the coast. When compared to the monthly AVHRR SST, the upwelling feature in the NCEP
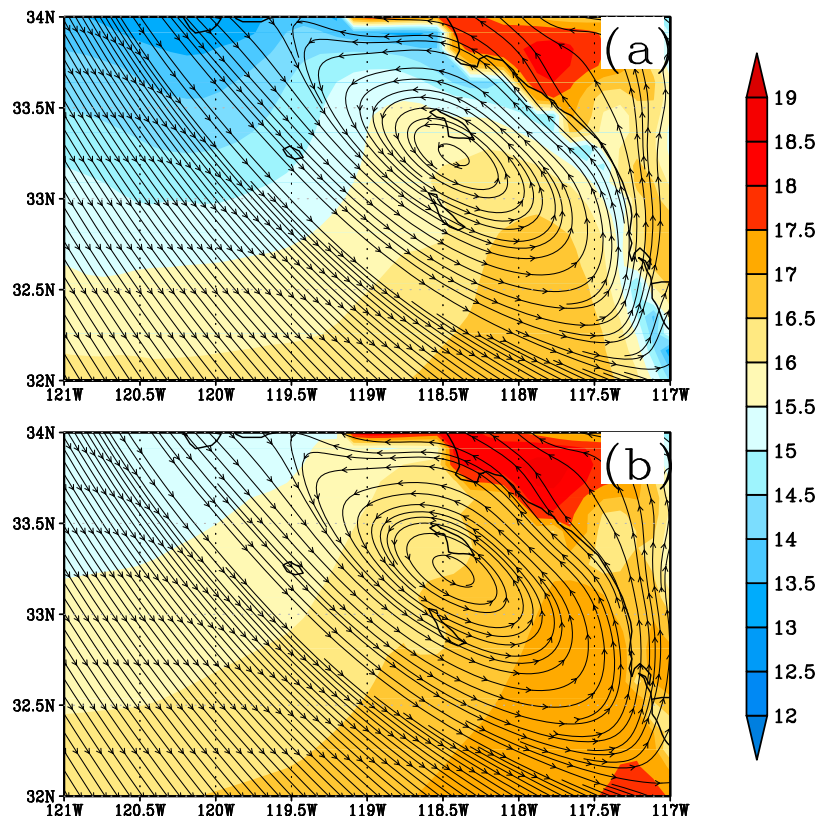

Figure 10. The composite Catalina Eddy from (a) CPL and (b) UNCPL. Shading is used to denote the surface air temperatures (°C).

SST is too weak, while the fine-scale features of the simulated SST are comparable to those from satellite observations. The daily variance in the NCEP SST is too small when compared to that for the buoy observations, but the CPL SST is higher than the buoy SST variance. In the summer, the temporal correlation of the NCEP SST against coastal buoy observations was improved by the CPL SST.

[48] The difference in the surface air temperature from the CPL and UNCPL runs is strongest in the summer upwelling season, particularly over the San Francisco Bay. The summer climatology temperature difference between the CPL and UNCPL experiments is $-1.11°C$ over San Francisco, while the inland city of Sacramento is cooled by $0.34°C$. The difference in the surface air temperature from the CPL and UNCPL experiments is not attributed to sea breeze, as the sea breeze difference over land is too small to have any significant meaning. The cold coastal CPL SST increases the stability of the planetary boundary layer and depresses the boundary height along the California coast by as much as 15% during the summer. The low cloud cover during the summer could be influenced by as much as 10% due to the coupling over the Central and Southern California coasts. This indicates that the SST influence can penetrate the boundary layer and reach the free atmosphere. Mesoscale circulation of the Catalina Eddy is enhanced by the coupling due to the colder SST along the coast of the Southern California Bight, and 6.5% more Catalina Eddy hours are detected in the CPL experiment when compared to UNCPL run.

[49] The performance of the coupled downscaling is reasonable, as it produces some better oceanic features (e.g., upwelling) than the one-degree coarse resolution NCEP SST. When validated against buoy observations, the CPL SST showed a certain level of statistical superiority over the daily time scale when compared to the NCEP SST. While the regional coupled model forced by the R-2 atmosphere and SODA oceanic reanalysis tends to generate a near-realistic ocean state, it has a relatively small impact on the atmospheric state. However, the impact is significant when the regional coupled model is forced by the projected global climate, which will be presented in a future study.

References

Boé, J., A. Hall, F. Colas, J. C. McWilliams, X. Qu, J. Kurian, and S. B. Kapnick (2011), What shapes mesoscale wind anomalies in coastal upwelling zones?, *Clim. Dyn.*, 36, 2037–2049, doi:10.1007/s00382-011-1058-5.

Carton, J. A., G. Chepurin, X. Cao, and B. S. Giese (2000), A simple ocean data assimilation analysis of the global upper ocean 1950–1995. Part I: Methodology, *J. Phys. Oceanogr.*, 30, 294–309, doi:10.1175/1520-0485(2000)030<0294:ASODAA>2.0.CO;2.

Centurioni, L. R., J. C. Ohlmann, and P. P. Niiler (2008), Permanent meanders in the California Current System, *J. Phys. Oceanogr.*, 38, 1690–1710, doi:10.1175/2008JPO3746.1.

Chelton, D. B., and S.-P. Xie (2010), Coupled ocean-atmosphere interaction at oceanic mesoscales, *Oceanogr. Mag.*, 23, 52–69, doi:10.5670/oceanog.2010.05.

Chelton, D. B., M. G. Schlax, and R. M. Samelson (2007), Summertime coupling between sea surface temperature and wind stress in the California Current System, *J. Phys. Oceanogr.*, 37, 495–517, doi:10.1175/JPO3025.1.

Chen, F., and J. Dudhia (2001), Coupling an advanced land-surface hydrology model with the Penn State/NCAR MM5 modeling system. Part I: Model implementation and sensitivity, *Mon. Weather Rev.*, 129, 569–585, doi:10.1175/1520-0493(2001)129<0569:CAALSH>2.0.CO;2.

Chou, M.-D., M. J. Suarez, C.-H. Ho, M. M.-J. Yan, and K.-T. Lee (1998), Parameterizations for cloud overlapping and shortwave single-scattering properties for use in general circulation and cloud ensemble models, *J. Clim.*, 11, 202–214, doi:10.1175/1520-0442(1998)011<0202:PFCOAS>2.0.CO;2.

Dickinson, R. E., R. M. Errico, F. Giorgi, and G. T. Bates (1989), A regional climate model for western United States, *Clim. Change*, 3, 383–422.

Di Lorenzo, E., A. J. Miller, N. Schneider, and J. C. McWilliams (2005), The warming of the California Current System: Dynamics and ecosystem implications, *J. Phys. Oceanogr.*, 35, 336–362, doi:10.1175/JPO-2690.1.

Giorgi, F., and G. T. Bates (1989), On the climatological skill of a regional model over complex terrain, *Mon. Weather Rev.*, 117, 2325–2347, doi:10.1175/1520-0493(1989)117<2325:TCSOAR>2.0.CO;2.

Giorgi, F., C. Shields Brodeur, and G. T. Bates (1994), Regional climate change scenarios over the United States produced with a nested regional climate model: Spatial and seasonal characteristics, *J. Clim.*, 7, 375–399, doi:10.1175/1520-0442(1994)007<0375:RCCSOT>2.0.CO;2.

Held, I. M., and B. J. Soden (2006), Robust responses of hydrological cycle to global warming, *J. Clim.*, 19, 5686–5699, doi:10.1175/JCLI3990.1.

Hickey, B. M. (1998), Coastal oceanography of western North America from the tip of Baja California to Vancouver Island, in *The Sea*, vol. 11, *Coastal Segment*, edited by A. R. Robinson and K. H. Brink, pp. 345–391, John Wiley, Hoboken, N. J.

Hong, S.-Y., and E. Kalnay (2000), Role of sea surface temperature and soil-moisture feedback in the 1998 Oklahoma-Texas drought, *Nature*, 408, 822–844.

Hong, S.-Y., and H.-L. Pan (1996), Nonlocal boundary layer vertical diffusion in a medium-range forecast model, *Mon. Weather Rev.*, 124, 2322–2339, doi:10.1175/1520-0493(1996)124<2322:NBLVDI>2.0.CO;2.

Hong, S.-Y., N.-K. Moon, K.-S. S. Lim, and J.-W. Kim (2010), Future climatic change scenarios over Korea using a multi-nested downscaling system: A pilot study, *Asia Pac. J. Atmos. Sci.*, 46, 425–435, doi:10.1007/s13143-010-0024-1.

Iacobellis, S. F., and R. C. J. Somerville (2000), Implications of microphysics for cloud-radiation parameterization: Lessons from TOGA COARE, *J. Atmos. Sci.*, 57, 161–183, doi:10.1175/1520-0469(2000)057<0161:IOMFCR>2.0.CO;2.

Juang, H.-M. H., and M. Kanamitsu (1994), The NMC nested regional spectral model, *Mon. Weather Rev.*, 122, 3–26, doi:10.1175/1520-0493(1994)122<0003:TNNRSM>2.0.CO;2.

Juang, H.-M. H., S.-Y. Hong, and M. Kanamitsu (1997), The NCEP regional spectral model: An update, *Bull. Am. Meteorol. Soc.*, 78, 2125–2143, doi:10.1175/1520-0477(1997)078<2125:TNRSMA>2.0.CO;2.

Kanamaru, H., and M. Kanamitsu (2007), Fifty-seven-year California Reanalysis Downscaling at 10km (CaRD10). Part II: Comparison with North American regional reanalysis, *J. Clim.*, 20, 5572–5592, doi:10.1175/2007JCLI1522.1.

Kanamitsu, M., and L. DeHaan (2011), The Added Value Index: A new metric to quantify the added value of regional models, *J. Geophys. Res.*, 116, D11106, doi:10.1029/2011JD015597.

Kanamitsu, M., and H. Kanamaru (2007), Fifty-seven-year California Reanalysis Downscaling at 10 km (CaRD10). Part I: System detail and validation with observations, *J. Clim.*, 20, 5553–5571, doi:10.1175/2007JCLI1482.1.

Kanamitsu, M., and K. Mo (2003), Dynamical effect of land surface processes on summer precipitation over the southwestern United States, *J. Clim.*, 16, 496–509, doi:10.1175/1520-0442(2003)016<0496:DEOLSP>2.0.CO;2.

Kanamitsu, M., W. Ebisuzaki, J. Woollen, S.-K. Yang, J. J. Hnilo, M. Fiorino, and G. L. Potter (2002), NCEP-DOE AMIP-II Reanalysis, *Bull. Am. Meteorol. Soc.*, 83, 1631–1643, doi:10.1175/BAMS-83-11-1631.

Kanamitsu, M., K. Yoshimura, Y.-B. Yhang, and S.-Y. Hong (2010), Errors of interannual variability and multi-decadal trend in dynamical regional climate downscaling, *J. Geophys. Res.*, 115, D17115, doi:10.1029/2009JD013511.

Kirtman, B. P. (2003), The COLA anomaly coupled model: Ensemble ENSO prediction, *Mon. Weather Rev.*, 131, 2324–2341, doi:10.1175/1520-0493(2003)131<2324:TCACME>2.0.CO;2.

Koo, M.-S., and S.-Y. Hong (2010), Diurnal variations of simulated precipitation over East Asia in two regional climate models, *J. Geophys. Res.*, 115, D05105, doi:10.1029/2009JD012574.

Large, W. G., J. C. McWilliams, and S. C. Doney (1994), Oceanic vertical mixing: A review and a model with a nonlocal boundary layer parameterization, *Rev. Geophys.*, *32*, 363–403, doi:10.1029/94RG01872.

Leung, L. R., Y. Qian, X. Bian, W. M. Washington, J. Han, and J. O. Roads (2004), Mid-century ensemble regional climate change scenarios for the western United States, *Clim. Change*, *62*(1–3), 75–113, doi:10.1023/B:CLIM.0000013692.50640.55.

Liang, X.-Z., L. Li, K. E. Kunkel, M. Ting, and J. X. L. Wang (2004), Regional climate model simulation of U.S. precipitation during 1982–2002. Part I: Annual cycle, *J. Clim.*, *17*, 3510–3529, doi:10.1175/1520-0442(2004)017<3510:RCMSOU>2.0.CO;2.

Marchesiello, P., J. C. McWilliams, and A. Shchepetkin (2003), Equilibrium structure and dynamics of the California Current System, *J. Phys. Oceanogr.*, *33*, 753–783, doi:10.1175/1520-0485(2003)33<753:ESADOT>2.0.CO;2.

Mellor, G. L., and T. Yamada (1982), Development of a turbulence closure model for geophysical fluid problems, *Rev. Geophys.*, *20*, 851–875, doi:10.1029/RG020i004p00851.

Mesinger, F., et al. (2006), North American Regional Reanalysis, *Bull. Am. Meteorol. Soc.*, *87*, 343–360, doi:10.1175/BAMS-87-3-343.

Miller, N. L., et al. (2009), An analysis of simulated California climate using multiple dynamical and statistical techniques, *CEC Rep. CEC-500-2009-017-F*, Calif. Energy Comm., Sacramento.

Reynolds, R. W., and T. M. Smith (1994), Improved global sea surface temperature analyses using optimum interpolation, *J. Clim.*, *7*, 929–948, doi:10.1175/1520-0442(1994)007<0929:IGSSTA>2.0.CO;2.

Russell, G. L., and D. Rind (1999), Response to CO_2 transient increase in the GISS coupled model: Regional coolings in a warming climate, *J. Clim.*, *12*, 531–539, doi:10.1175/1520-0442(1999)012<0531:RTCTII>2.0.CO;2.

Saha, S., et al. (2006), The NCEP Climate Forecast System, *J. Clim.*, *19*, 3483–3517, doi:10.1175/JCLI3812.1.

Seo, H., A. J. Miller, and J. O. Roads (2007a), The Scripps Coupled Ocean-Atmosphere Regional (SCOR) model, with applications in the eastern Pacific sector, *J. Clim.*, *20*, 381–402, doi:10.1175/JCLI4016.1.

Seo, H., M. Jochum, R. Murtugudde, A. J. Miller, and J. O. Roads (2007b), Feedback of tropical instability wave–induced atmospheric variability onto the ocean, *J. Clim.*, *20*(23), 5842–5855, doi:10.1175/JCLI4330.1.

Seol, K.-H., and S.-Y. Hong (2009), Relationship between the Tibetan snow in spring and the East Asian summer monsoon in 2003: A global and regional modeling study, *J. Clim.*, *22*, 2095–2110, doi:10.1175/2008JCLI2496.1.

Shchepetkin, A. F., and J. C. McWilliams (2005), The Regional Ocean Modeling System: A split-explicit, free-surface, topography following coordinates ocean model, *Ocean Modell.*, *9*, 347–404, doi:10.1016/j.ocemod.2004.08.002.

Shimpo, A., M. Kanamitsu, S. F. Iacobellis, and S.-Y. Hong (2008), Comparison of four cloud schemes in simulating the seasonal mean field forced by the observed sea surface temperature, *Mon. Weather Rev.*, *136*, 2557–2575, doi:10.1175/2007MWR2179.1.

Song, H., A. J. Miller, B. D. Cornuelle, and E. Di Lorenzo (2011), Changes in upwelling and its water sources in the California Current System driven by different wind forcing, *Dyn. Atmos. Oceans*, *52*, 170–191, doi:10.1016/j.dynatmoce.2011.03.001.

Song, Y. T., and D. B. Haidvogel (1994), A semi-implicit ocean circulation model using a generalized topography following coordinate system, *J. Comput. Phys.*, *115*, 228–244, doi:10.1006/jcph.1994.1189.

Souma, K., and Y. Wang (2009), Improved simulation of the East Asian summer monsoon rainfall with satellite-derived snow water equivalent data, *Mon. Weather Rev.*, *137*, 1790–1804, doi:10.1175/2008MWR2800.1.

Stowasser, M., Y. Wang, and K. P. Hamilton (2007), Tropical cyclone changes in the western North Pacific in a global warming scenario, *J. Clim.*, *20*, 2378–2396, doi:10.1175/JCLI4126.1.

Sun, L., D. F. Moncunill, H. Li, A. D. Moura, D. A. Francisco, D. S. Filho, and S. E. Zebiak (2006), An operational dynamical downscaling prediction system for nordeste Brazil and the 2002–04 real-time forecast evaluation, *J. Clim.*, *19*(10), 1990–2007, doi:10.1175/JCLI3715.1.

Taylor, K. E., D. Williamson, and F. Zwiers (2000), The sea surface temperature and sea ice concentration boundary conditions of AMIP II simulations, *PCMDI Rep. 60*, 20 pp., Lawrence Livermore Natl. Lab., Livermore, Calif.

Tiedtke, M. (1993), Representation of clouds in large-scale models, *Mon. Weather Rev.*, *121*, 3040–3061, doi:10.1175/1520-0493(1993)121<3040:ROCILS>2.0.CO;2.

Ulrickson, B. L., J. S. Hoffmaster, J. Robinson, and D. Vimot (1995), A numerical modeling study of the Catalina Eddy, *Mon. Weather Rev.*, *123*, 1364–1373, doi:10.1175/1520-0493(1995)123<1364:ANMSOT>2.0.CO;2.

Umlauf, L., and H. Burchard (2003), A generic length-scale equation for geophysical turbulence models, *J. Mar. Res.*, *61*, 235–265, doi:10.1357/002224003322005087.

Vecchi, G. A., and B. J. Soden (2007), Global warming and the weakening of the tropical circulation, *J. Clim.*, *20*, 4316–4340, doi:10.1175/JCLI4258.1.

Xie, S.-P., T. Miyama, Y. Wang, H. Xu, S. P. de Szoeke, R. J. Small, K. J. Richards, T. Mochizuki, and T. Awaji (2007), A regional ocean-atmosphere model for eastern Pacific climate: Towards reducing tropical biases, *J. Clim.*, *20*, 1504–1522, doi:10.1175/JCLI4080.1.

Yhang, Y.-B., and S.-Y. Hong (2008), Improved physical processes in a regional climate model and their impact on the simulated summer monsoon circulations over East Asia, *J. Clim.*, *21*, 963–979, doi:10.1175/2007JCLI1694.1.

Yoshimura, K., and M. Kanamitsu (2009), Specification of external forcing for regional model integrations, *Mon. Weather Rev.*, *137*, 1409–1421, doi:10.1175/2008MWR2654.1.